Chimeric a-subunit isoforms generate functional yeast V-ATPases with altered regulatory properties *in vitro* and *in vivo*

Farzana Tuli and Patricia M. Kane*

Dept. of Biochemistry and Molecular Biology

SUNY Upstate Medical University

Syracuse, NY

*To whom correspondence should be addressed: kanepm@upstate.edu

ABSTRACT

V-ATPases are highly regulated, multi-subunit proton pumps that acidify organelles. The V-ATPase a-subunit is a two-domain protein containing a C-terminal transmembrane domain that participates in proton transport and a N-terminal cytosolic domain (aNT) that acts as a regulatory hub, integrating environmental inputs to regulate assembly, localization, and V-ATPase activity. Tissue- and organelle-specific a-subunit isoforms exist in most organisms, but how regulatory inputs are decoded by aNT isoforms is unknown. The yeast *S. cerevisiae* encodes only two organelle-specific a-isoforms, Stv1 in the Golgi and Vph1 in the vacuole. Based on recent structures, we designed chimeric yeast aNTs in which the globular proximal and distal ends are exchanged. The Vph1 proximal-Stv1 distal (VPSD) aNT chimera binds to the glucose-responsive RAVE assembly factor *in vitro* but exhibits little binding to phosphoinositide lipids that activate V-ATPases. The Stv1 proximal-Vph1 distal (SPVD) aNT lacks RAVE binding but binds more tightly to phosphoinositides than Vph1 or Stv1. When attached to the Vph1 C-terminal domain *in vivo*, both chimeras complement growth defects of a *vph1*Δ mutant, but only the SPVD chimera exhibits wild-type V-ATPase activity. Cells containing the SPVD chimera adapt more slowly to a poor carbon source than wild-type cells but grow more rapidly than wild-type after a shift to alkaline pH. This is the first example of a "redesigned" V-ATPase with altered regulatory properties and adaptation to specific stresses.

INTRODUCTION

The intracellular compartments of eukaryotic cells maintain a unique pH range which is critical for their function (Casey et al., 2010). The organelles of the secretory and endocytic pathways become progressively more acidic, with the lysosome/vacuole as the most acidic organelle (Huotari & Helenius, 2011). All acidic compartments in these pathways possess Vacuolar H^+-ATPases (V-ATPases) which acidify their lumen. In addition, some specialized cells have plasma membrane V-ATPases that secrete H^+ into the extracellular space. V-ATPases play important roles in many cellular processes including vesicular transport, neurotransmitter loading, ion homeostasis, urine acidification, and bone resorption (Breton & Brown, 2013; Collins et al., 2020; Eaton et al., 2021; Forgac, 2007). Consistent with their diverse roles in cell physiology, aberrant activity of V-ATPases has been associated with many pathological conditions such as osteopetrosis (Frattini et al., 2000), renal tubular acidosis (Smith et al., 2000) and metastatic cancer (Sennoune et al., 2004). However, complete loss of V-ATPase activity is lethal in higher eukaryotes (Sun-Wada et al., 2003), which makes therapeutic targeting of V-ATPases very difficult (Kane, 2012).

V-ATPases are ATP hydrolysis-driven proton pumps that are conserved from yeast to humans. These multi-subunit protein complexes consist of two main subcomplexes where the cytosolic, peripheral complex, V_1, hydrolyzes ATP and membrane-bound complex, V_o, contains the proton pore (Forgac, 2007). V-ATPases undergo different modes of regulation to fine tune their activity depending on cellular need (Forgac, 2007). One major mechanism of regulation of activity is by reversible disassembly where the V_1 and V_o sectors reversibly disassemble in response to many signals such as upon glucose deprivation (Kane, 1995) (Sumner et al., 1995). Signal-dependent disassembly of V_1 from V_o leads to the inactivation of both ATP hydrolysis (Parra et al., 2000) and proton pumping (Couoh-Cardel et al., 2015). Significant conformational changes of the disassembled V_1 and V_o complexes prevent reassembly when enzyme activity is not needed. The RAVE (Regulator of acidification in vacuole and endosome) complex is required for rapid reassembly of yeast V-ATPase *in vivo* (Seol et al., 2001). V-ATPase activity can also be modulated by phosphatidylinositol phosphate (PIP) lipids (Banerjee et al., 2019; Vasanthakumar et al., 2019) which are enriched in organelle membranes and may stabilize the assembled conformation of V-ATPase. In addition, isoforms of many V-ATPase subunits allow for tissue-specific and organelle-specific regulation. How isoform composition endows V-ATPases with distinct catalytic and regulatory properties is poorly understood.

The a-subunit from the V_o sector is encoded by multiple tissue- and organelle-specific isoforms in most eukaryotic cells. In yeast, the only V-ATPase subunit isoforms are in the V_o a-subunit and are encoded by the *VPH1* and *STV1* genes. Vph1-containing V-ATPases are enriched in the vacuole (Manolson et al., 1992) , and Stv1-containing V-ATPases localize to the Golgi (Manolson et al., 1994). These isoforms determine localization of their respective complexes and confer different catalytic and regulatory properties. In all eukaryotes, a-subunit isoforms consist of a cytosolic N-terminal domain (NT) and a membrane bound C-terminal domain (CT). Chimeras of yeast a-subunits containing NT and CT of the opposite isoforms revealed that the NT domain encodes information for localization and reversible disassembly (Kawasaki-Nishi et al., 2001). Subsequent studies showed that the NT domains also dictate binding to different organelle-enriched phosphoinositide lipids (Banerjee et al., 2019; Banerjee & Kane, 2017; Li et al., 2014). The overall backbone structure of the NT domain of all a-subunit isoforms is predicted to be similar, with 50% identity and 70% similarity at the amino acid level.

Cryo-EM structures reveal that the aNT domains are characterized by a proximal end (which connects to the aCT domain) and a distal end; the two ends are connected by a long coiled-coil. Recent structures of Vph1-containing V_o and Stv1-containing V_o revealed strong similarity in overall structure but failed to resolve poorly conserved loops at both proximal and distal ends of aNTs (Vasanthakumar et al., 2019). These loops are likely flexible and may contribute to unique catalytic and regulatory properties of the isoforms. Indeed, sequences from these loop regions have previously been implicated in lipid binding (Banerjee et al., 2019; Banerjee & Kane, 2017).

The aNT domain is an important regulatory hub of V-ATPase for several reasons. First, it occupies a critical position at the V_1-V_o interface **(Figure 1A)**. It undergoes significant conformational changes in the V-ATPase holoenzyme vs. disassembled V_o subcomplexes (Couoh-Cardel et al., 2015). Second, the proximal and distal ends form quaternary interactions with different V_1 subunits (Oot & Wilkens, 2012; Sharma et al., 2018); these interactions must be supported by all isoforms to preserve V-ATPase assembly and activity. Third, the aNT harbors many different regulatory interactions. Cellular factors important for V-ATPase regulation such as the RAVE complex (Smardon et al., 2014), PIP lipids (Banerjee et al., 2019; Banerjee & Kane, 2017; Li et al., 2014), glycolytic enzymes (Lu et al., 2007; Su et al., 2008), and the Rab-GEF protein ARNO (Hurtado-Lorenzo et al., 2006) all interact with aNT domains. However, it is not well understood where the information for these regulatory interactions resides in the aNT domains.

Here, we aimed to understand where two of the regulatory interactions, RAVE and PIP lipids, reside in the aNT domain and how the information from these two inputs is integrated to control V-ATPase activity. Toward this goal, we have constructed chimeric aNTs by swapping the proximal and distal ends between Vph1 and Stv1. *In vitro* studies with the resulting chimeras suggest that the information for RAVE binding resides in the proximal end of Vph1NT. Lipid binding experiments suggest that multiple sequences in Stv1NT from both ends promote PI(4)P binding. Unlike previous chimeric a-subunits, a chimera containing proximal end of Stv1 in combination with distal end of Vph1 assembles into fully functional V-ATPases in vacuoles when attached to the Vph1 C-terminal domain. However, the altered regulatory properties of this chimera have significant physiological consequences for yeast cells.

RESULTS

Design and expression of chimeric and mutant proteins

In order to better understand the regulatory information embedded in the cytosolic aNT domains, we generated chimeras of Vph1NT and Stv1NT by swapping the proximal and distal ends between the two isoforms **(Figure 1B, C)**. Although medium resolution cryo-EM structures of intact V-ATPases containing both Vph1 (Benlekbir et al., 2012; Zhao et al., 2015) and Stv1 (Vasanthakumar et al., 2019) are available, there are regions of the aNT domains that are missing from the structures or poorly resolved, including the regions previously implicated in lipid binding (Banerjee et al., 2019; Banerjee & Kane, 2017). We generated high confidence homology models of Vph1NT (1-372) and Stv1NT (1-418) to help identify potential locations for the junctions in the chimeras (**Figure 1B)**. As shown in **Figure 1B** both isoforms have a similar coiled-coil backbone between the two globular domains. Pairwise alignment of the two isoforms helped identify conserved regions in the coiled-coil that might be suitable as a junction.

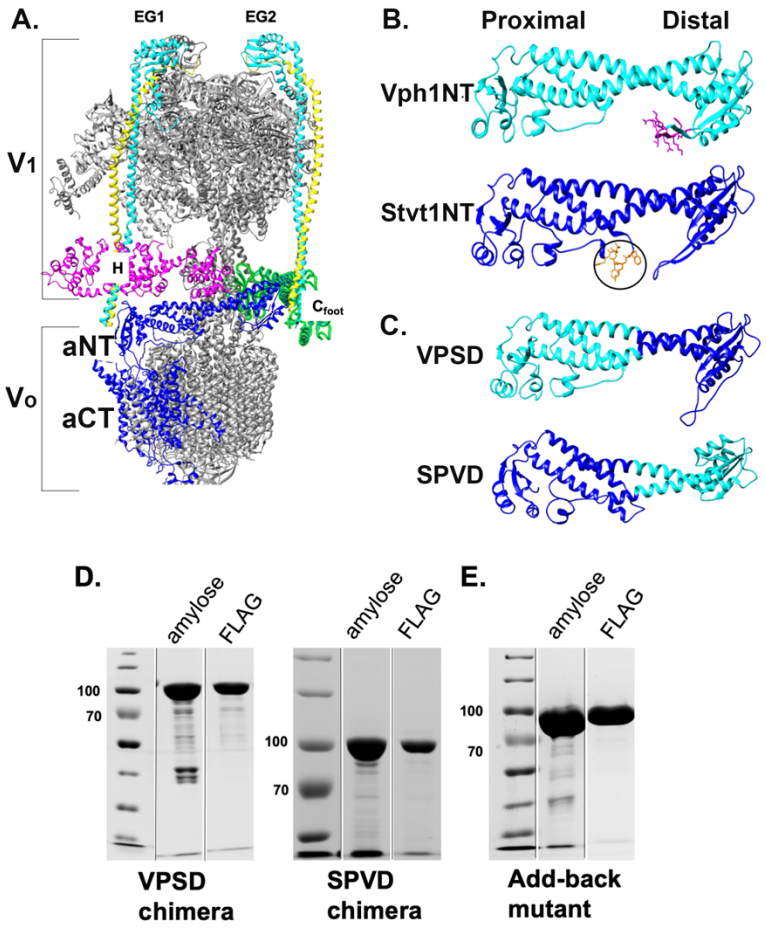

Figure 1: Design and construction of chimeric and mutant a-NT's. A. Cryo-EM structure (3.1-Å resolution) of human V-ATPase holoenzyme (PDB 6WM2) where aNT is shown in dark blue polypeptide chain. Subunits interact with aNT domain are represented in color; V_1 E1 and E2-teal, V_1 G1 and G2-yellow, V_1 H-purple, V_1 C_{foot} -green. **B.** Phyre2 generated homology models of yeast Vph1NT (aa. 1-372) and Stv1NT (aa. 1-418) with the proximal and distal ends indicated. Amino acids previously implicated in PI(3,5)P_2 activation of Vph1-containing ATPases are indicated on Vph1NT in magenta, and the amino acids implicated in PI(4)P binding to Stv1 are shown in yellow and circled. **C.** Schematic diagram of chimeric proteins constructed by swapping the two ends between the isoforms. **D, E.** Coomassie stained SDS–PAGE showing MBP-tagged VPSD and SPVD chimeras and add-back mutant after the first (amylose) and second (anti-FLAG) affinity purification steps. Lines indicate positions where non-adjacent lanes from the same gel were moved together.

Finally, we placed the junction in a region of high sequence similarity in the middle of the coiled-coil. Although this region binds to the V_1 H subunit in the fully assembled complex (Vasanthakumar et al., 2019), both Stv1 and Vph1 interact with subunit H, suggesting that a hybrid would also support the interaction. Importantly, exchange at this junction is predicted to preserve the structures of the two ends. The resulting chimeras were designated $Vph1NT_{proximal}$ $Stv1NT_{distal}$ (VPSD chimera) and $Stv1NT_{proximal}$ $Vph1NT_{distal}$ (SPVD chimera) **(Figure 1C).** VPSD chimera carries amino acids 1-123 of Vph1NT, 133-342 of Stv1NT and 295-372 of Vph1NT, whereas the SPVD chimera carries residues 1-132 of Stv1NT, 124-294 of Vph1NT and 343-418 of Stv1NT. In addition to these chimeras, we constructed an "add-back mutant" in which we added the Stv1NT W83KYILH sequence containing the identified PI(4)P recognition site (Banerjee & Kane, 2017; Finnigan et al., 2012) into the corresponding loop of the Vph1NT proximal domain (**Figure 1B**, shown in circle).

The chimeric and mutant aNT proteins were expressed in E. coli with a N-terminal maltose binding protein (MBP) tag and a C-terminal FLAG tag and purified through sequential amylose then anti-FLAG affinity chromatography **(Figure 1D, E)** followed by gel filtration. The

127 gel filtration profile of the chimeric and mutant proteins **(Figure 1-Supp. Figure S1)** was very
128 similar to that of the wild-type aNTs, including the characteristic monomer-dimer peak that is
129 observed for wild-type Vph1NT and Stv1NT (Banerjee & Kane, 2017; Oot & Wilkens, 2012).
130 The monomer fractions were used in the subsequent assays.

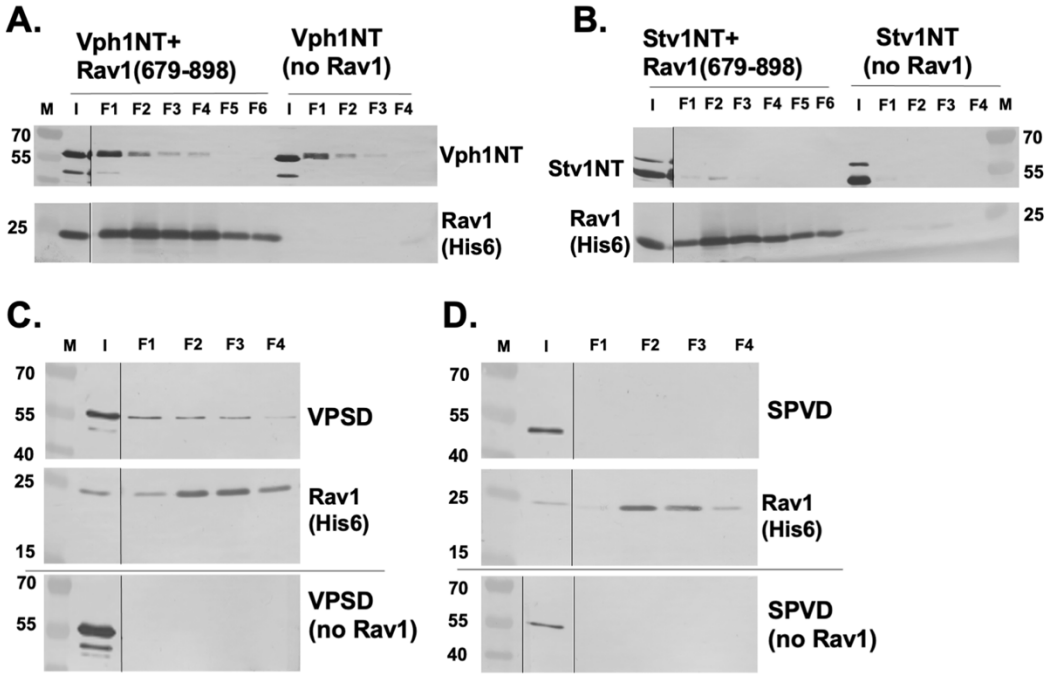

131

132

Figure 2: The proximal end of Vph1NT binds to Rav1 (679-898). Vph1NT, Stv1NT, and the VPSD and SPVD chimeras were expressed and purified as in Figure 1 except that the MBP tag was removed with Prescission protease. Rav1 (679-898)-His_6 was expressed and purified as described (Smardon et al., 2014). The aNT proteins were mixed with the Rav1 (679-898) at a 5:1 molar ratio. The mixtures were added to TALON resin and incubated at 4°C for 2 h. to allow binding. The pull-down assay was performed as described (Jaskolka & Kane, 2020). The Rav1 (679-898) fragment was used to pull-down: **A.** Vph1NT, **B.** Stv1NT, **C.** VPSD and **D.** SPVD, and the bound proteins eluted with imidazole in the indicated fractions. For each pull-down assay the indicated protein was also mixed with TALON resin in absence of Rav1 (no Rav1 control). Anti-FLAG monoclonal antibody was used to probe for Vph1NT, Stv1NT, VPSD and SPVD while anti-His_6 antibody was used to probe Rav1 (679-898). Lines indicate positions where non-adjacent lanes from the same gel were moved together. M: molecular mass markers, I: input.

133

134 **The proximal end of Vph1NT binds to Rav1 (679-898)**

135 The yeast RAVE complex is an isoform-specific assembly factor required only for the
136 assembly of Vph1-containing V-ATPases; Stv1-containing V-ATPases can assemble
137 independently of RAVE (Smardon et al., 2014). Vph1NT directly interacts with one RAVE
138 subunit, Rav1, in two-hybrid and pull-down assays (Smardon et al., 2014; Smardon et al., 2015)
139 (Jaskolka & Kane, 2020). A central fragment of Rav1 (aa 679-898) has a binding site for

Vph1NT (Smardon et al., 2015) and point mutations and small deletions in this region abolish recruitment of RAVE to the vacuolar membrane *in vivo* (Jaskolka & Kane, 2020). Expressed Vph1NT co-elutes with a Rav1(679-898)His_6 fragment from TALON resin (**Figure 2A**). As described previously, (Jaskolka & Kane, 2020) there is a small amount of Vph1NT present in a control lacking Rav1 but it is less than that in the presence of the Rav1 fragment, suggesting the interaction is specific. In contrast, no coelution of Stv1NT with Rav1(679-898)His_6 was observed in similar pull-down assay **(Figure 2B)**. Although these experiments support isoform-specific binding, chimeric aNTs provide an opportunity to narrow down the RAVE binding domain. We performed similar pull-down assays with the Rav1(679-898)His_6 fragment and chimeric aNTs. We found that the VPSD chimera coeluted with Rav1(679-898) His_6 **(Figure 2C)** and there was no VPSD chimera detected in the no Rav1 control, indicating the interaction is specific. In contrast, the SPVD chimera, which lacks the proximal end of Vph1NT, did not coelute with Rav1(679-898) His_6 fragment **(Figure 2D)**. In the SPVD chimera, the proximal end of Vph1 is replaced with the proximal end of Stv1NT but the distal end of Vph1NT is present. These data suggest that the Vph1 proximal end present in the VPSD chimera has the information for binding to this critical region of Rav1, whereas the distal end is not important for this interaction.

Transfer of PIP specificity between aNT isoforms

Recently, it has become clear that PIP lipids interact with V-ATPase isoforms and contribute to their activity, localization, and regulation (Banerjee et al., 2019; Banerjee & Kane, 2017; Li et al., 2014). We tested binding of the chimeric yeast aNT constructs to PI(4)P and PI(3,5)P_2 in a quantitative liposome pelleting assay (Chandra et al., 2019). Liposomes with or without phosphoinositide were incubated with a defined concentration of the aNT protein. Liposomes and bound protein were isolated by centrifugation as described in Materials and Methods, and binding was assessed by measuring the proportion of total protein in the pellet. PIP-specific binding was determined by subtracting the protein bound in the absence of phosphoinositide from that bound in the presence of phosphoinositide. All of the proteins were tested for pelleting in the absence of lipid, and none pelleted, indicating that the presence of protein in the pellet was liposome-dependent.

Stv1NT binds to Golgi-enriched PI(4)P *in vivo* and to PI(4)P-containing liposomes in a liposome flotation assay (Banerjee & Kane, 2017). Mutation of K84, located in the proximal end of Stv1NT, abolished binding to PI(4)P-containing liposomes *in vitro*, suggesting this region is necessary for lipid binding. However, it was not determined whether this region is sufficient for PI(4)P interaction, and the contribution of other regions of Stv1NT to lipid binding is not known. As shown in **Figure 3A**, **B** Stv1NT showed much more binding to PI(4)P liposomes than Vph1NT at a protein concentration of 0.5 μM. We tested whether we could transfer Stv1NT PI(4)P specificity to Vph1NT by constructing an "add-back mutant" in which we added the W83KYILH sequence containing the K84 residue from Stv1 (**Figure 1B**, shown in circle) at a similar position in Vph1NT. As shown in **Figure 3A**, **B**, the add-back mutant bound to PI(4)P liposomes comparably to Stv1NT and significantly better than Vph1NT at the lower protein concentration. However, the SPVD chimera, in which the entire proximal end domain of Vph1NT was replaced with Stv1NT, bound even more strongly to PI(4)P suggesting that other sequences in the Stv1NT proximal domain can strongly enhance binding **(Figure 3A, B, C)**. The VPSD chimera, in which the entire distal end domain of Vph1NT was replaced with the distal end of Stv1NT also showed significantly better binding than Vph1NT alone at 0.5 μM protein

185 **(Figure 3A, B, C)**. Together these data support the previously identified K84-containing
186 sequence as a major PI(4)P binding site in Stv1 which is sufficient to transfer PI(4)P binding to
187 Vph1NT. However, results with the chimeras indicate that both the entire proximal and the distal
188 ends of Stv1NT also have sequences that can further promote PI(4)P binding.

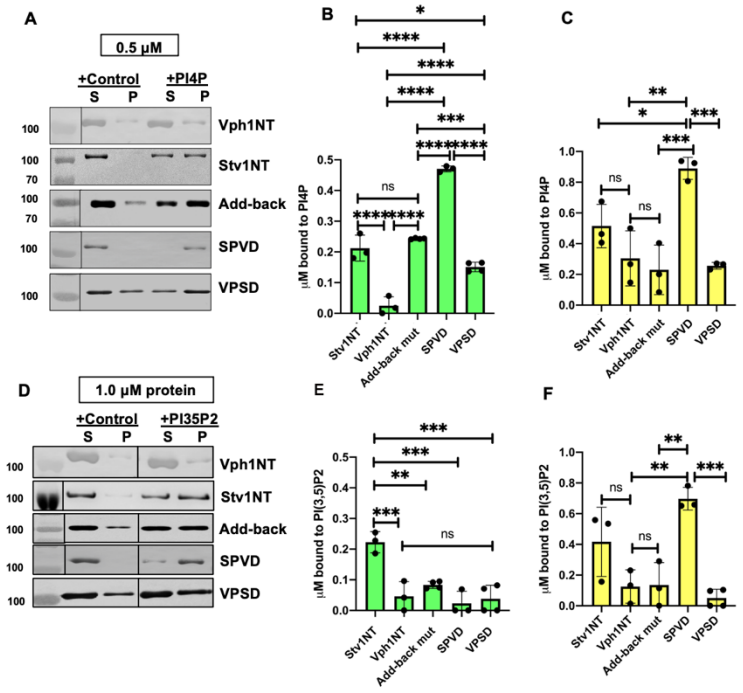

189

Figure 3: PIP lipid binding of chimeric and mutant aNTs in liposome pelleting assays. Liposomes were prepared as described (Banerjee & Kane, 2017). All proteins were expressed and purified as in Figure 1. Protein solutions at a final concentration of either 0.5 μM or 1 μM were incubated with control (no PIP), 5% PI(4)P or 5% PI(3,5)P_2 containing liposomes (final concentration of 0.33 mM) in separate centrifuge tubes as described in *Materials and Methods*. Following centrifugation, the supernatant (S) were collected, and pellet (P) fractions were resuspended in 100 μl of 50 mM Tris-Cl, 100 mM NaCl (pH 7.4) before TCA precipitation and analysis by SDS-PAGE and immunoblotting with anti-FLAG antibody. **A., D.** Representative immunoblots showing distribution of the indicated proteins between the supernatant (S) and pellet (P) pellet fractions with control and PIP-containing liposomes. **A.** 0.5μM of each protein with control and PI(4)P-containing liposomes, **B.** 1 μM of each protein with control and PI(3,5)P_2 containing liposomes. In A and B, vertical lines represent movement of non-adjacent lanes from the same gel next to each other. **B, C, E, F.** At least three assays were performed for each protein-liposome combination and band intensities were determined using ImageJ. PIP-specific binding was determined by subtracting the proportion of total protein bound in the control pellets from the proportion in the PIP pellet, then multiplying by the total protein concentration to get PIP-specific binding. Bar graphs show the average concentration of each protein bound specifically to liposomes containing the indicated PIP lipid. **B, C.** PI(4)P-specific binding at total protein concentrations of 0.5μM **(B)** and 1μM **(C)**. **E, F.** PI(3,5)P_2-specific binding at total protein concentrations of 0.5μM **(E)** and 1μM **(F)**. Error bars represent standard deviation. In each graph, binding for each protein was compared to every other protein by ordinary one-way ANOVA with Tukey's multiple comparison test; significant differences between the strains are indicated: ****, P<0.0001 ***, P<0.0005; **, P<0.005; *, P<0.05; ns, P>0.05

190 Direct *in vitro* interaction between the vacuolar isoform Vph1NT and PI(3,5)P_2 has not
191 been observed previously. However, addition of exogenous PI(3,5)P_2 specifically enhances the
192 ATPase and proton pumping activities of Vph1-containing V-ATPases in isolated vacuolar
193 vesicles and this enhancement is abolished by mutations in the Vph1 distal domain (Banerjee et
194 al., 2019). In addition, Vph1NT shows PI(3,5)P_2-dependent recruitment to membranes *in vivo*
195 (Li et al., 2014). We tested binding of Vph1NT and the chimeric proteins to PI(3,5)P_2-containing
196 liposomes in a liposome pelleting assay under similar conditions to those used with PI(4)P-
197 containing liposomes (i.e. 0.5 µM protein). Vph1NT pelleted poorly with PI(3,5)P_2 liposomes
198 **(Figure 3D, E)** and there was no significant difference in binding between Vph1NT and the add
199 back mutant or chimeras under these conditions. We also conducted the assay in the presence of
200 1 µM protein **(Figure 3E)**. At the higher protein concentration, the SPVD chimera, which
201 contains the Stv1NT proximal domain and the Vph1NT distal domain, showed significantly
202 higher binding than Vph1NT, the add-back mutant or VPSD chimera. The low affinity of
203 Vph1NT for PI(3,5)P_2 is not surprising, as this is a regulatory interaction predicted to allow
204 activation at high PI(3,5)P_2 concentrations. However, it was surprising that Stv1NT bound as
205 well to PI(3,5)P_2 as it did to PI(4)P, even though it shows a preference for PI(4)P in the previous
206 flotation assay and exhibited PI(4)P-dependent recruitment to membranes *in vivo* (Banerjee &
207 Kane, 2017). The overall strong lipid binding of the SPVD chimera may arise from sequences
208 the distal domain of Vph1NT previously implicated in PI(3,5)P_2 activation in combination with
209 PIP lipid binding sequences in the proximal domain of Stv1NT.

210 **Expression of chimeric aNTs in yeast**

211

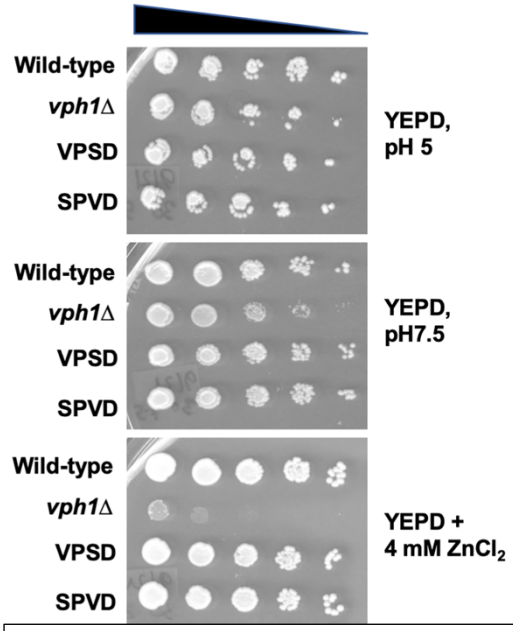

Although the expressed aNT domains are optimal for *in vitro* assays, they do not capture the full function of the aNT domains *in vivo*, where they are tethered in proximity to membranes by attachment to the integral membrane aCT domains and must bind to multiple V-ATPase subunits. To compare their functions as part of a full-length a subunit, chimeric aNT sequences were integrated into *VPH1,* replacing the Vph1NT sequence and placing them under control of *VPH1* promoter. The resulting strain still has wild-type Stv1 localized to the Golgi and would be expected to express the chimeric a-subunits at higher levels than *STV1* since the *VPH1* promoter is much stronger (Kawasaki-Nishi et al., 2001; Manolson et al., 1994). We performed growth assays to assess V-ATPase function in the yeast strains containing chimeric a-

Figure 4: Growth complementation by chimeric aNTs combined with Vph1CT. The VPSD and SPVD chimeric aNTs were integrated into the yeast genome, replacing Vph1NT, to generate VPSD and SPVD mutant strains. Growth of wild-type, VPSD and SPVD strains were compared to that of a *vph1*Δ strain by growing each strain to log phase in YEPD pH 5, diluting to an A_{600} of 0.8 then serially diluting 10-fold in a microtiter plate. Cells were transferred to YEPD pH 5, YEPD pH 7.5 and YEPD Zn^{2+} plates and grown for 3 days at 30°C.

228 subunits. Mutants lacking V-ATPase activity grow best at pH 5. Loss of Vph1 function makes
229 yeast sensitive to high extracellular pH and elevated level Zn^{2+} concentrations (Manolson et al.,
230 1994) as shown for the *vph1*Δ mutant in **Figure 4**. However, both chimeric aNT mutations were
231 well tolerated *in vivo*, as they both complement the growth defects of the *vph1*Δ mutant **(Figure**
232 **4).**
233
234 **The V-ATPases containing SPVD chimera are fully assembled and active**

235 We isolated vacuolar vesicles from wild-type cells and the strains containing the SPVD
236 and VPSD chimeras and measured V-ATPase activity and assembly at the vacuole. Vacuolar
237 vesicles from the VPSD chimera had significantly less V-ATPase activity than the wild-type or
238 SPVD vesicles (**Figure 5A).** In order to better understand the source of the defect in the VPSD
239 vesicles, we compared the levels of the V_1 subunits A, B, and C, V_o subunit d, and control
240 vacuolar membrane protein ALP between the vesicle preparations. Although alkaline
241 phosphatase (ALP) levels are similar between the vesicle preparations, indicating comparable
242 purity, all of the V_1 subunits and V_o subunit d are at lower levels in the VPSD vesicles,
243 suggesting a V-ATPase assembly or stability defect **(Figure 5B)**. The chimeric a-subunits
244 showed different interactions with antibodies against Vph1 and Stv1. One of the monoclonal
245 antibodies (7B1H1) raised against yeast vacuolar membranes (Kane et al., 1992) not only
246 recognized Vph1 as expected, but also cross-reacted with the SPVD chimera. In contrast, another
247 monoclonal antibody (10D7) only recognized Vph1 and VPSD, but not SPVD. A polyclonal
248 antibody against Stv1 recognized VPSD and SPVD but not Vph1.

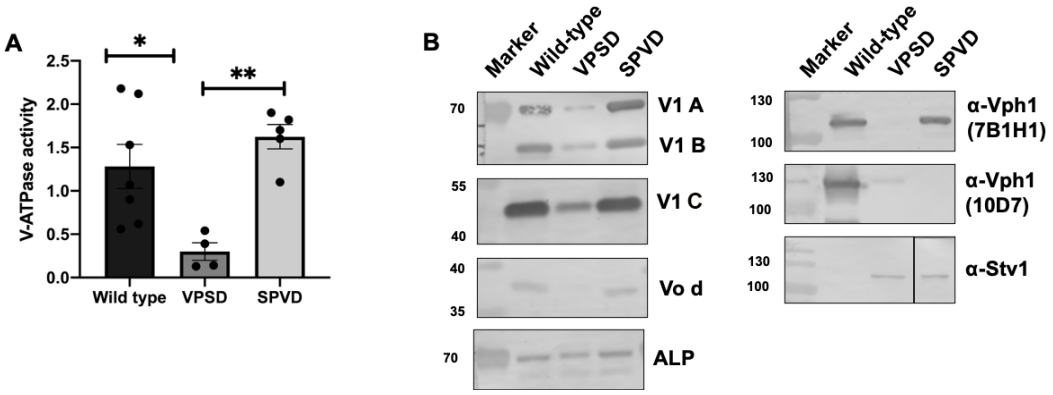

249

Figure 5: The V-ATPases containing SPVD chimera are active and fully assembled: Vacuolar vesicles were isolated from wild-type cells and cells containing the VPSD and SPVD chimera. **A.** V-ATPase–specific activity (defined as the activity sensitive to 100 nM concanamycin A and expressed as μmol/min/mg protein) was measured for at least four independent preparations of vacuolar vesicles, and the mean ± SEM is shown. **B.** The vesicles were solubilized, separated by SDS-PAGE, transferred to nitrocellulose, and probed with antibodies against V_1 subunits A, B, and C, V_o subunit d, or alkaline phosphatase (ALP), a vacuolar integral membrane protease. Vesicles were also probed with two monoclonal antibodies specific for Vph1 (7B1H1 and 10D7) as well as polyclonal antisera against Stv1; none of these antibodies could detect the a-subunit from all three strains. For the detection of A- and B-subunits 2.5 μg of vacuolar protein was loaded. 10 μg of protein was loaded to detect a and C subunits, and 7.5 μg of protein was loaded for visualization of a-subunits and alkaline phosphatase.

In contrast to the VPSD chimera, vesicles from the SPVD chimera had a mean ATPase activity slightly higher than those from wild-type cells, although the difference in activity was not statistically significant. The levels of V_1 subunits in the SPVD vacuolar vesicles were also as high, or slightly higher, as in wild-type vesicles, and the V_o d-subunit was at similar levels. We also measured proton pumping in the wild-type and SPVD vesicles in order to assess the coupling ratio (the ratio of the initial rate of proton pumping to the initial rate of ATP hydrolysis) and found that the ratios were very similar between wild-type and SPVD vesicles (data not shown). In summary, despite differences in regulatory properties, the SPVD mutant is as assembled and active as the wild-type V-ATPase. This is remarkable because previous chimeras of Stv1 and Vph1, including one containing the entire Stv1NT in combination with Vph1CT, had assembly defects and less than 30% of wild-type activity (Kawasaki-Nishi et al., 2001).

The SPVD chimera is partially independent of RAVE function

The RAVE complex plays roles in both biosynthetic assembly of the V-ATPase and reassembly after disassembly induced by glucose deprivation. *rav1*Δ mutants have very low V-ATPase activity and assembly in vacuoles (Smardon et al., 2002), so it was somewhat surprising that the SPVD chimera, which appears to lack Rav1 binding**,** had such high activity and assembly. We investigated the degree of RAVE independence of SPVD chimera by making a genomic deletion of *RAV1* in this mutant. The *rav1*Δ mutants grow well at pH 5 but grow poorly in media containing 4 mM Zn^{2+} or elevated pH and calcium even at 30°C (Seol et al., 2001; Smardon et al., 2002). We found that the *rav1*ΔSPVD chimera grew as well as wild type at high pH and calcium concentration and quite well in zinc-containing medium at 30°C **(Figure 6)**. The growth defect of *rav1*ΔSPVD mutants is milder than *rav1*Δ mutants indicating that V-ATPases containing the SPVD chimera are at least somewhat independent of RAVE.

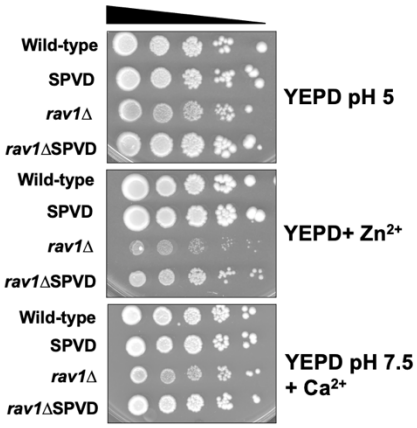

Figure 6: The SPVD chimera is partially independent of RAVE. Growth phenotypes of wild- type, SPVD, *rav1*Δ and *rav1*ΔSPVD strains were tested by growing strains to log phase in YEPD pH 5, diluting to an A_{600} of 0.8 and serially diluting 10-fold in a microtiter plate. Cells were transferred by pinning to YEPD pH 5 and YEPD + 4 mM $ZnCl_2$ (YEPD +Zn^{2+}) plates and grown for 3 days at 30°C. Cells transferred to YEPD pH 7.5 + 60 mM $CaCl_2$ (YEPD pH 7.5 +Ca^{2+}) plates were grown for 5 days at 30°C.

Is there a physiological cost of the SPVD mutation?

Although V-ATPases containing the SPVD chimera appear to be fully assembled and functional, our *in vitro* experiments suggest that their regulatory properties may be quite different than those of wild-type V-ATPases. Reversible disassembly is a major regulatory mechanism for V-ATPases (Oot et al., 2017). In yeast, it is likely to be particularly important under conditions of acute glucose deprivation (Parra & Kane, 1998). We first checked whether V-ATPase regulation by reversible disassembly is retained in the SPVD chimera. We performed immunoprecipitations from whole cell lysates of wild-type and the SPVD chimera maintained in

the presence of glucose, after 20 min of glucose deprivation, and 20 min after glucose readdition to the glucose-deprived cells. A monoclonal antibody against the V_1 subunit B was previously shown to immunoprecipitate both V_1 subcomplexes and fully assembled V_1-V_o complexes (Doherty & Kane, 1993; Smardon et al., 2002). We used this antibody to immunoprecipitate these complexes from both strains and assessed the ratio of V_1 to V_o by comparing levels of V_1 B-subunits to their respective V_o a-subunit, then calculating the percent assembly relative to the starting (+glucose) samples.

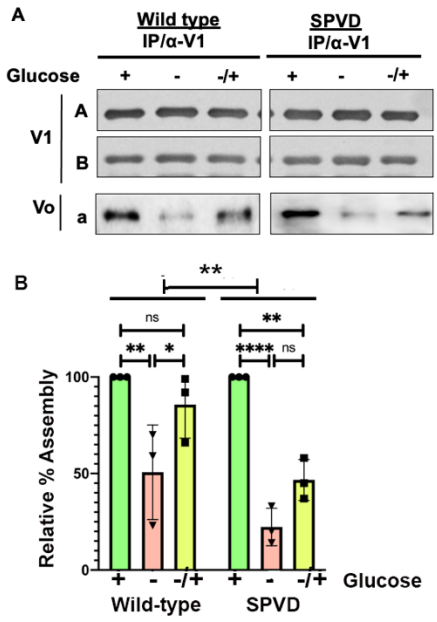

Figure 7: Glucose-dependent disassembly and reassembly in wild-type and SPVD cells
A. Immunoprecipitation of V-ATPases from wildtype and SPVD from spheroplast lysates was performed as described in (Kane, 1995) and Materials and Methods. Yeast cells were converted to spheroplasts, which were then incubated for 30 min in YEP media with (+) or without (-) 2% glucose. A third sample (-/+) was incubated without glucose for 20 min followed by 30 min incubation with 2% glucose. V-ATPases were immunoprecipitated under each condition using the monoclonal antibody 13D11 against the V_1 B-subunit followed by Protein A-Sepharose. Immunoprecipitated proteins were subjected to SDS-PAGE and transferred to nitrocellulose. Western blot analysis was performed using primary antibody 8B1F3 (against the V_1 A-subunit), 13D11 (against the V_1 B-subunit), 7B1H1 (against Vph1NT) or polyclonal anti-Stv1 antisera. Dissociation of the V-ATPase complex is reflected as a decrease in the amount of a-subunit immunoprecipitated. A representative experiment from three separate replicates is shown. **B.** Bar diagram showing mean assembly under each condition, relative to the assembly each strain maintained in glucose of wild type and SPVD cells. Error bars represent standard deviation. Comparison between the strains was performed by two-way ANOVA (without multiple comparison). Results for +glucose, -glucose and glucose addback (-/+) conditions were also compared for each strain by two-way ANOVA with Tukey's multiple comparison test. Significance of differences is indicated as: ****, $P<0.0001$; ***, $P<0.0005$; **, $P<0.005$; *, $P<0.05$; ns, $P>0.05$

There are significant differences in the behavior of the two strains **(Figure 7A, B)**. V-ATPases in the SPVD disassemble more completely than those in the wild-type strain (a mean of 22% relative assembly vs. 51% in wild-type). Rapid reassociation of disassembled V_1 and V_o after glucose readdition to glucose-deprived cells requires the RAVE complex *in vivo* (Seol et al., 2001). In wild type cells, the ratio of V_1 to V_o was rapidly restored to a mean of 86% of the pre-deprivation level after glucose readdition **(Figure 7B)**. In the SPVD chimera the average assembly after glucose addition was less than 50% of the pre-deprivation level **(Figure 7B)**. Together, these data suggest that V-ATPases in SPVD chimera disassemble more extensively during glucose deprivation and cannot reassemble completely after a short time of glucose readdition.

Reversible disassembly of V-ATPases may help support cell growth by preserving ATP during the periods of deprivation that arise during shifts in carbon source. We tested how cells containing the SPVD chimera adjust during a transition to a less preferred carbon source. Wild

type and SPVD mutant cells were grown to log phase in YEPD (glucose) medium and diluted into fresh medium containing glucose or raffinose, then growth was analyzed for next 24 hr. Both strains exhibited similar growth rates in medium containing 2% glucose as shown in **Figure 8A**, but the SPVD strain had a somewhat longer lag before growth initiation. There was a longer lag in growth of wild-type cells upon a shift to raffinose; this is not unexpected because both transcriptome and proteome changes occur during a shift to raffinose metabolism (Paulo et al., 2015). Interestingly, SPVD cells have a significantly longer lag than wild type cells when shifted to raffinose than when shifted to glucose-containing medium. These data indicate that with SPVD mutation cells cannot as readily adjust to changes in carbon sources as wild-type cells, consistent with the incomplete V-ATPase reassembly in **Figure 7B**.

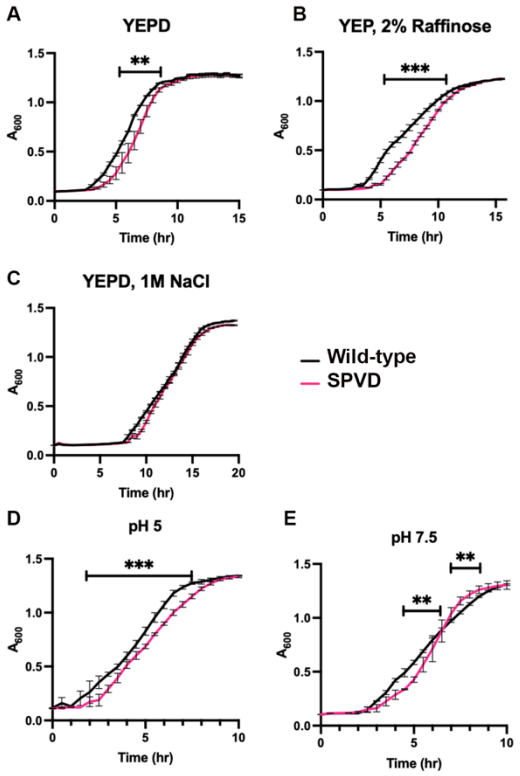

Figure 8: Growth of SPVD mutant under stress conditions. A-C. The wild-type and SPVD mutant strains were grown to log phase in YEPD, then diluted into the indicated medium to a density of A_{600}=0.1. Growth was then monitored for 24 hr. at 30°C. Growth curves for wild type and SPVD strains in **A.** YEPD (YEP containing 2% glucose) **B.** 2% raffinose (YEP containing 2% raffinose) **C.** 1.0 M NaCl (YEPD containing 1 M NaCl) **D, E.** Wild-type and SPVD strains were grown to log phase in YEPD buffered to pH 5, then diluted into: **D.** pH 5 (YEPD buffered to pH 5) or **E.** pH 7.5 (YEPD buffered to pH 7.5). Growth was observed over the span of 24 hr at 30°C. Mean growth rates ± S.D. from three independent experiments are shown. Multiple t-tests were performed and significant differences in growth between the strains are indicated: ***, P<0.0005, **, P<0.005; all other differences were not significant.

PI(3,5)P_2 is a signaling lipid that helps cells to adapt to multiple stresses (Jin et al., 2017; McCartney et al., 2014). Mutants lacking PI(3,5)P_2 are sensitive to high salt (Bonangelino et al., 2002) and *vph1* mutants defective in PI(3,5)P_2 activation also exhibit salt-dependent phenotypes (Banerjee et al., 2019; Bonangelino et al., 2002). We hypothesized that the SPVD chimera might have an advantage after a shift to medium containing high salt because it shows tighter binding to PI(3,5)P_2. However, cells containing wild-type *VPH1* or the SPVD chimera showed very similar lags and growth rates **(Figure 8C)**. Under alkaline growth conditions, V-ATPase activity is increased and the enzyme shows little disassembly upon glucose deprivation (Diakov & Kane, 2010); this stabilization at alkaline pH is dependent on PI(3,5)P_2 (Li et al., 2014). We hypothesized that increased PI(3,5)P_2 binding of the SPVD chimera might provide a growth benefit when cells are shifted from low to high pH_{ext} (pH 5 to pH 7.5). The SPVD mutant again had a somewhat longer lag when diluted into pH 5 medium **(Figure 8D)**. However, at pH 7.5 the SPVD cells grew at a significantly faster rate than wild type cells after the initial lag (**Figure**

336 **8E**). These data indicate that the different regulatory interactions of the wild-type and SPVD
337 aNT domains *in vitro* may also affect the response of cells to distinct stresses *in vivo*.
338
339 **DISCUSSION**
340
341 The cytosolic aNT domains of V_o a-subunit isoforms occupy a critical location at the
342 interface of the V_1 and V_o subcomplexes and have long been recognized as a major locus of
343 regulation. It is also clear that different a-subunit isoforms endow V-ATPases with distinct
344 regulatory capacities. However, where regulatory responses reside in the aNT domains of
345 different isoforms and how they decode distinct regulatory signals are not completely
346 understood.

347 The aNT chimeras help define isoform-specific regulation in more detail. Binding of the
348 Rav1(678-898) fragment to the VPSD chimera suggests that the specificity for RAVE binding,
349 which is linked to the isoform-specific reversible disassembly of Vph1-containing V-ATPases
350 (Smardon et al., 2014), resides in the proximal end of Vph1NT. This region of Rav1 is critical
351 for recruitment of RAVE to the vacuolar membrane, as mutations in a small conserved sequence
352 in the center completely prevent recruitment (Jaskolka & Kane, 2020). The RAVE complex has
353 been proposed to template reassembly of the V-ATPase, and the proximal end of Vph1NT may
354 be a "landing site" for the RAVE complex bearing the V_1 subcomplex and subunit C that could
355 then orient the complexes for reassembly of the active complex (Jaskolka et al., 2021). Binding
356 of RAVE to the proximal end of Vph1NT could leave the distal end free to assemble a
357 quaternary complex with the foot domain of subunit C and the appropriate EG peripheral stalk,
358 which is likely to be a critical step in reassembly (Oot et al., 2017). Alternatively, binding of the
359 proximal domain to RAVE could help pull Vph1NT into the more peripheral position seen in the
360 V-ATPase holoenzyme from the collapsed position adjacent to V_o subunit d seen in the
361 disassembled V_o (Stam & Wilkens, 2017).

362 Although interactions of aNT isoforms with PIP lipids have been investigated previously,
363 experiments with the chimeric aNTs provide new insights. Interestingly, potential lipid binding
364 sites have been identified in poorly conserved loops of both the proximal domain (Stv1NT)
365 (Banerjee & Kane, 2017) and the distal domain (Vph1NT) (Banerjee et al., 2019), suggesting
366 both ends of the aNT domain can potentially contribute to PIP binding and altered V-ATPase
367 activity. Consistent with previous results, we find that Vph1NT acquires PI(4)P binding *in vitro*
368 upon addition of the lysine 84-containing sequence from Stv1NT. However, both the SPVD
369 chimera, which contains this sequence, and the VPSD chimera, which does not, show better
370 binding to PI(4)P than Vph1NT, suggesting that other Stv1NT sequences can contribute to
371 PI(4)P binding. Previous attempts to determine direct interaction between Vph1NT and PI(3,5)P_2
372 in a liposome flotation assay were unsuccessful, and poor binding was also observed in the
373 liposome pelleting assay used here **(Figure 3)**. This is not surprising, because PI(3,5)P_2 binding
374 to Vph1NT appears to be a reversible, regulatory interaction *in vivo* (Li et al., 2014), and thus
375 may be tuned to a lower affinity. In contrast to previous results from liposome flotation assays,
376 Stv1NT showed similar binding to PI(4)P and PI(3,5)P_2 in the liposome pelleting assay in
377 **Figure 3,** despite its strong preference for PI(4)P *in vivo* (Banerjee & Kane, 2017). Binding in
378 the flotation assay is strongly influenced by off-rates, while the pelleting assay is an equilibrium
379 assay. Interestingly, the SPVD chimera, which contains both of previously determined PIP
380 binding sites, binds more tightly to both PI(4)P and PI(3,5)P_2 than either Stv1NT or Vph1NT *in*

381 *vitro*. Cryo-EM structures indicate that both the proximal and distal domains of the aNTs
382 collapse toward the center of the disassembled, inactive V_o sector (Mazhab-Jafari et al., 2016;
383 Roh et al., 2018). When the aNT is part of an intact a-subunit, lipid binding to either end could
384 help stabilize the subunit in a more peripheral configuration optimal for assembly and activity.
385 Thus, PIP binding to both ends of the SPVD chimera could potentially provide even greater
386 stability.

387 The SPVD chimera is the first fully functional chimera of Stv1 and Vph1. Kawasaki-
388 Nishi et al. constructed chimeras containing the entire NT domain of Stv1 and Vph1 in
389 combination with the CT domains of the opposite isoform (Kawasaki-Nishi et al., 2001).
390 However, both of those chimeras had <30% of the activity and assembly than the wild-type
391 enzyme, comparable to the 23% of wild-type activity in the VPSD mutant (**Figure 5A**). In
392 contrast, the activity, coupling, and assembly of the SPVD chimera in isolated vacuolar vesicles
393 is at least as good as those of the wild-type enzyme. This indicates that binding of the RAVE
394 complex to the proximal end of the chimeric aNT is either not essential for the biosynthetic
395 assembly V-ATPases containing the SPVD chimera, or that the proximal end of Stv1NT is
396 sufficient to support RAVE-independent biosynthesis. Stv1-containing V-ATPases can assemble
397 in the absence of RAVE, so this capability may be carried in the Stv1NT proximal end.
398 However, it is also interesting to speculate that the increased lipid binding to SPVD-containing
399 ATPases might circumvent the need for RAVE in biosynthetic assembly. In addition to its
400 biosynthetic role, RAVE is required for reassembly after glucose deprivation (Seol et al., 2001;
401 Smardon et al., 2002). The SPVD chimera actually disassembles to a greater extent than the
402 wild-type V-ATPase upon glucose deprivation, so it is difficult to determine whether there is any
403 specific defect in reassembly with glucose readdition. Biosynthetic assembly and reassembly
404 occur by different pathways, so RAVE interactions may differ between the two pathways (Kane,
405 2006).

406 The SPVD chimera provides novel insights into how V-ATPases integrate isoform-
407 specific regulatory inputs to achieve physiological responses. PIP binding and reversible
408 disassembly are associated with V-ATPase responses to different stresses (Kane, 1995; Li et al.,
409 2012), and their regulatory effects are separable. Reversible disassembly in response to glucose
410 deprivation still occurs in the absence of vacuolar $PI(3,5)P_2$, suggesting that this process is
411 independent of PIP binding (Li et al., 2014). However, V-ATPases responses to glucose are
412 strongly RAVE-dependent. V-ATPase disassembly can occur with acute glucose deprivation,
413 from exhaustion of glucose during growth, and in transitions to poor carbon sources (Kane,
414 1995; Parra & Kane, 1998). We found that despite having wild-type activity in isolated vacuoles,
415 the SPVD mutant was slow to resume growth after a shift from glucose to the poor carbon source
416 raffinose **(Figure 8B**). Thus, even if the SPVD chimera does not require RAVE for its initial
417 assembly, interaction with the RAVE complex may be critical for cells to readjust to shifts in
418 carbon source. In other physiological situations, RAVE binding may be less important. Vacuolar
419 $PI(3,5)P_2$ is implicated in stabilization and/or activation of assembled V-ATPases at the vacuole
420 under high salt and alkaline growth conditions (Diakov & Kane, 2010; Li et al., 2014). The
421 increased $PI(3,5)P_2$ binding to the SPVD chimera did not provide a growth advantage when cells
422 were shifted to high salt (**Figure 8C**). However, $PI(3,5)P_2$ stabilization of V-ATPases under
423 alkaline stress could help explain the higher growth rate of SPVD mutant at pH 7.5, after an
424 initial lag (**Figure 8E**). Further experiments will be needed to fully define the underlying

425 mechanism, but this is the first example of a chimeric V-ATPase with a growth advantage over
426 wild-type under specific stress conditions.

427 Total loss of V-ATPase activity is lethal in higher eukaryotes (Sun-Wada et al., 2003), so
428 targeting isoform-specific functions and regulatory mechanisms is an attractive route for
429 therapeutic modulation of V-ATPase activity. Generation of functional V-ATPases with altered
430 regulatory properties provides a means to better understand both the mechanism and underlying
431 balance of isoform-specific regulation. Importantly, our results indicate that it may be possible to
432 retain full V-ATPase activity under basal conditions, thus avoiding lethality, while changing the
433 enzyme's regulation and cellular responses to stress.
434
435

436 **MATERIALS AND METHODS**

437 ***Materials, media and cell growth***

438 Amylose and TALON resin were purchased from New England Biolabs and Clontech,
439 respectively. Anti-FLAG M2 resin, mouse anti-FLAG antibody, and FLAG peptide were
440 purchased from Sigma. Lipids were purchased as lyophilized powder from Avanti Polar Lipids.
441 Sepharose A beads were purchased from GE Healthcare. DSP (dithiobis (succinimidyl
442 propionate)) crosslinker was obtained from Pierce.

443 Liquid medium for E. coli culture consisted of 2.5% Luria–Bertani broth (LB), Miller
444 powder (Fisher BioReagents). For expression of proteins from E. coli 0.2% dextrose was added
445 to LB. To maintain plasmids carrying an ampicillin- or chloramphenicol resistance genes, we
446 added 125 µg/ml ampicillin (Sigma-Aldrich) or 34 µg/ml chloramphenicol (Sigma-Aldrich),
447 respectively.

448 Yeast cells were grown on rich media containing 1% yeast extract, 2% peptone and 2%
449 dextrose (YEPD). YEPD was buffered to pH 5.0 or pH 7.5 by 50 mM potassium phosphate and
450 50 mM potassium succinate. For plates with added $CaCl_2$, YEPD was buffered to pH 7.5 with 50
451 mM Mes (2-(N-morpholino) ethanesulfonic acid) 50 mM MOPS (3-(N-morpholino)
452 propanesulfonic acid) buffer, and 60 mM $CaCl_2$ was added (YEPD, pH 7.5, Ca^{2+}). YEPD+Zn^{2+}
453 containing plates consisted of 4 mM $ZnCl_2$ in unbuffered YEPD. YEPD+G418 contained 200
454 µg/ml G418 (Gibco Genticin, Thermo Fisher Scientific). For auxotrophic selections, fully
455 supplemented minimal medium with 2% dextrose (SD) lacking individual nutrients was used.
456 Yeast cells were grown to log phase in indicated media and collected near A_{600}=1 for
457 transformation as described (Gietz & Schiestl, 2007). For dilution growth assays, the indicated
458 wild-type or mutant yeast cells were grown to log phase in YEPD, pH 5. Cell suspensions were
459 adjusted to a single density, and 10-fold serial dilutions were made and then pinned onto the
460 desired plates.

461 ***Cloning, expression and purification of MBP-Vph1NT(1-372)-FLAG, VPSD chimera, SPVD***
462 ***chimera and add-back mutant***

463 MBP-Vph1NT(1-372)-FLAG: A single FLAG tag was inserted at the C-terminus of
464 MBP-Vph1NT (1-372) by TA cloning. Specifically, Vph1NT nucleotide sequence 1-1116
465 carrying a 5' BamH1 and a 3' FLAG was PCR amplified using oligonucleotides Vph1NT
466 5'BamH1 and Vph1NT 3'FLAG (Table 2) and a template of MBP-Vph1NT (1-372) plasmid

467 DNA. After addition of a non-templated A, the PCR product was then ligated in pGEM T-easy
468 vector. Subsequently, BamH1-Vph1NT-FLAG was cloned into pMal c2E Precision protease
469 vector that had been cut with restriction enzymes BamHI and PstI.

470 The VPSD chimera carrying amino acid residues 1-123 of Vph1NT, 133-342 of Stv1NT
471 and 295-372 of Vph1NT was generated by using a megaprimer PCR technique (Forloni et al.,
472 2019). A sequence of Vph1NT corresponding to amino acid 124-294 was replaced with sequence
473 corresponding to Stv1NT amino acid 133-342 using oligonucleotides Stv1NT 133F and Stv1NT
474 324R and a template of MBP-Vph1NT (1-372)-FLAG plasmid DNA.

475 The SPVD chimera carrying amino acid residues 1-132 of Stv1NT, 124-294 of Vph1NT
476 and 343-418 of Stv1NT was generated by using similar megaprimer PCR technique. A sequence
477 of Stv1NT corresponding to amino acid 133-342 was replaced with sequence corresponding to
478 Vph1NT amino acid 124-294 using oligonucleotides Vph1NT 124F and Vph1NT 294R and a
479 template of MBP-Stv1NT(1-418)-FLAG plasmid DNA.

480 For the add-back mutant, a mutant Vph1NT carrying Stv1NT W83KYILH amino acid
481 was generated by using oligonucleotide W83 Vph1F and Stv1W83Vph1R and a template of
482 MBP-Vph1NT (1-372)-FLAG plasmid DNA.

483 MBP-Vph1NT(1-372)-FLAG, MBP-Stv1NT(1-418)-FLAG, VPSD chimera, SPVD
484 chimera, add-back mutant and MBP-Rav1 (679-898)-His_6 cell were expressed, induced and
485 affinity purified on amylose columns as described previously (Jaskolka & Kane, 2020). All the
486 constructs were expressed in Rosetta competent cells (F^- *ompT hsdS*$_B$(r_B^- m_B^-) *gal dcm* (DE3)
487 pRARE (Cam^R)) (Novagen). To induce protein expression 0.5mM isopropyl B-D-
488 thiogalactopyranoside was added to cells when they reached a density of 0.5-0.6 OD/ml, and
489 growth was continued for 16 hr at 18°C. Proteins were affinity purified on amylose columns. A
490 second round of affinity purification was performed using anti-FLAG M2 Affinity resin. Peak
491 fractions were pooled, and 5 mM DTT was added immediately. After concentration to at least 1
492 mg/ml, the proteins were run on a Sephadex 200 (S200) gel-filtration fast protein liquid
493 chromatography (FPLC) column on an AKTA FPLC system. The peak corresponding to the
494 monomeric molecular mass was collected and used for additional experiments.

495 ***Pull-down assay***

496 Protein pull-down assays were performed as described (Jaskolka & Kane, 2020). The
497 only exception is that the two step affinity purified peak fractions of MBP-Vph1NT(1-372)-
498 FLAG, MBP-Stv1NT(1-418)-FLAG, VPSD chimera, SPVD chimera and pooled peak fractions
499 of Rav1 (679– 898)-His_6 from amylose column were dialyzed overnight in TALON equilibration
500 buffer. MBP was cleaved from the proteins with Prescission protease before affinity purification
501 on the FLAG column.

502 ***Liposome preparation and liposome pelleting assay***

503 Control liposomes and liposomes of defined PIP lipid contents are prepared as described
504 (Banerjee & Kane, 2017). For pelleting assays, the protein of interest was mixed with a final
505 volume of 100 µl of control (0% PIP) or experimental (5% PIP) liposomes to give a final
506 concentration of protein of 0.5 or 1 µM, and final total lipid concentration of 0.33 mM. The
507 mixtures were left at room temperature for 30 min to allow for protein–liposome interaction.
508 After incubation, the solution was centrifuged at 400,000 g for 30 min at 4°C in a TLA-100 fixed

509 angle rotor using a Beckman Coulter mini-ultracentrifuge. Supernatant and pellet fractions were
510 separated, and the pellet was resuspended in 100 µl of 50 mM Tris-Cl, 100 mM NaCl (pH 7.4).
511 Samples were then precipitated using 10% trichloroacetic acid. The pellets were washed with
512 cold acetone and dissolved in 50 µl of cracking buffer (50 mM Tris-HCl, pH 6.8, 8 M urea, 5%
513 SDS, and 1 mM EDTA). 25 µl of each sample were then separated by SDS-PAGE and
514 transferred into nitrocellulose membrane. The resulting blots were then probed with anti-FLAG
515 M2 antibody, followed by alkaline phosphatase-conjugated anti-mouse antibody. A no liposome
516 control was also performed to ensure that the protein of interest did not pellet on its own. For
517 these samples, the protein was diluted to final volume of 100 µl in the same buffer and subjected
518 to centrifugation and SDS-PAGE as described above.

519 A least three separate pelleting assays were performed for each protein concentration and
520 liposome type. Immunoblots were analyzed using ImageJ to quantitate intensity of the
521 supernatant and pellet bands which was subsequently converted to percentage of the total
522 (supernatant + pellet). For each experiment, the percentage of protein in the control (no PIP)
523 pellets were subtracted from that in the PIP pellets and the resulting value of specific binding
524 was multiplied by the total protein concentration to determine the PIP-specific binding. The
525 mean and standard deviation across replicates were calculated, and significance was determined
526 using Ordinary one-way ANOVA with multiple comparisons using GraphPad Prism 9.

527 ***Yeast strains***

528 The genotype of the strains used in this study are listed in Table 1.

529 For genomic integration of the VPSD chimeric aNT into full length *VPH1* under the
530 *VPH1* promoter, a fragment containing VPSD chimera was PCR amplified from the expression
531 plasmid described above using oligonucleotides SIV F and SIV R. This amplified PCR product
532 was then transformed into a strain in which Vph1NT sequence for amino acids 50-300 had been
533 replaced with *URA3* (Banerjee et al., 2019). Transformants capable of growth in presence of 5-
534 fluoro-orotic acid (FOA) were selected, analyzed for replacement of the *URA3* gene, and
535 sequenced to confirm introduction of the chimera sequence.

536 For genomic integration of SPVD chimeric aNT into full length *VPH1* under the *VPH1*
537 promoter, a plasmid containing 400 bp upstream of the *VPH1* open reading frame followed by
538 the SPVD chimera and 400 bp corresponding to Vph1CT amino acids 406-539 cloned into
539 pBluescript II KS(-) vector using BamHI and XhoI was purchased from Genscript. After
540 restriction digestion with BamH1 and Xho1, the fragment was then transformed into 5Aα Vph1
541 aa 50-300Δ::*URA3* strain and transformants were selected on FOA plates as described above.

542 To delete *RAV1* from the SPVD-containing yeast strain, nucleotide sequence of *URA3*
543 with ends homologous to *RAV1* was PCR amplified from a strain containing *rav1*Δ::*URA3* strain
544 using oligonucleotides rav1 Ura3F and Rav1 Ura3R. This amplified fragment was used to
545 transform 5Aα SPVD cells and transformants were selected on SD lacking uracil. Colony PCR
546 was performed to isolate transformants with the *RAV1* deletion.

547 ***Vacuole isolation and biochemical analysis***

548 Vacuoles were isolated as described in (Li et al., 2014). Purified vacuolar vesicles were
549 tested for ATPase activity in a coupled ATPase enzyme assay as described in (Liu et al., 2005)
550 except that the cuvettes containing reaction mixture were preheated at 37°C. To assess V-

551 ATPase specific activity, concanamycin A was added to a final concentration of 200 nM. Protein
552 concentration was determined by Lowry assay (Lowry et al., 1951) to determine V-ATPase
553 specific activity. Proton pumping was observed using the 9-amino-6-chloro-2-methoxyacridine
554 quenching assay described previously (Liu et al., 2005). 20 µg of vacuolar vesicles were used for
555 each assay. Pumping was initiated by adding 0.5 mM ATP and 1.0 mM MgSO4.

556 Western blots of vacuolar proteins were performed as in (Li et al., 2014). Mouse
557 monoclonal antibodies 8B1F3 and13D11 were used against V_1 subunits A and B (Kane et al.,
558 1992). Vph1 was detected using mouse monoclonals 7B1H1 and 10D7 (Kane et al., 1992).
559 Alkaline phosphatase was detected with mouse monoclonal 1D3A10 (Invitrogen). Rabbit
560 polyclonal antisera, a generous gift from Tom Stevens, University of Oregon, were used to detect
561 V_1 C and V_o d and SPVD (via anti-Stv1p antisera). Representative immunoblots were scanned to
562 obtain images used for figures.

563 ***Immunoprecipitation***

564 Immunoprecipitation was performed as described in (Kane, 1995) with the following
565 modifications. For each immunoprecipitation, volumes of cell culture equivalent to 20 OD_{600}
566 units were pelleted then converted to spheroplasts. The spheroplasts were incubated for 30 min
567 in YEP, 1.2 M sorbitol media with (+) or without (-) 2% glucose at 30°C. A third sample (-/+)
568 was incubated without glucose for 20 min followed by 30 min incubation with 2% glucose. The
569 spheroplasts were lysed, then complexes immunoprecipitated using the monoclonal antibody
570 13D11 against the B-subunit followed by Protein A Sepharose beads (Sigma). After elution with
571 cracking buffer, (8M urea, 50mM Tris HCL pH 6.8, 5% SDS, 1mM EDTA, 5% β-
572 mercaptoethanol) samples were vortexed and incubated for 20 min at 55°C. All samples were
573 then subjected to SDS-PAGE and transferred to nitrocellulose. Western blot analysis was
574 performed using primary antibody 8B1F3 (V_1 A-subunit), 13D11 (V_1 B-subunit), 7B1H1 (Vph1
575 in wild type) and anti-Stv1 antibody (SPVD). Alkaline phosphatase conjugate secondary
576 antibody was used for the detection of Vph1 in wild type whereas HRP conjugate secondary
577 antibody was used for the detection of the SPVD a-subunit. The extent of V-ATPase assembly
578 was assessed from the ratio of V_o to V_1 and normalized to ratio in the sample maintained in
579 glucose.

580 ***Growth curve assay***

581 For growth assays, yeast strains were grown overnight in YEPD and diluted to a density
582 of A_{600} = 0.05 in YEP containing 2% dextrose or 2% raffinose or YEPD containing 1 M NaCl. In
583 order to compare pH effects on growth, cells were grown overnight in YEPD buffered to pH 5,
584 then diluted to YEPD buffered to pH 5 or pH 7.5 as indicated. Growth over time was then
585 monitored on a SpectraMax i3X multi-mode multiplate reader for 24 hr.

586

587 ***Protein structure prediction***

588 The homology models of Vph1NT (1-372) and Stv1NT (1-448) were obtained by
589 submitting the corresponding amino acid sequences of Phyre2 server (Kelley et al., 2015). From
590 the submitted sequence, 100% confidence models based on Vph1NT in the state 1 rotational
591 structure of the yeast V-ATPase (Zhao et al., 2015) (PDB 3j9t) were obtained with 93%
592 coverage (Vph1NT 1-372) and 88% coverage (Stv1NT 1-418). Structures were visualized using
593 UCSF Chimera (Pettersen et al., 2004).

ACKNOWLEDGEMENTS

This work was supported by NIH R01 GM126020 to P.M.K. The authors thank Julianna Bourgeios and Maureen Tarsio for excellent technical help, Dr. Tom Stevens (University of Oregon) for antibodies, and Stephan Wilkens and his lab (Upstate Medical University) for helpful discussion and use of their FPLC.

COMPETING INTERESTS

The authors declare no competing interests.

Strains	Descriptions	Reference
SF838 5Aα	*Matα leu2-3, 112; ura3-52; ade6 gal2*	
*vph1*Δ	SF838 5Aα *vph1*Δ:: *LEU2*	(Zhao et al., 2015)
vph1 aa 50-300Δ	SF838 5Aα Vph1 aa 50-300Δ::*URA3*	(Banerjee et al., 2019)
VPSD	SF838 5Aα Vph1NT$_{proximal}$ Stv1NT$_{distal}$-Vph1CT	This study
SPVD	SF838 5Aα Stv1NT$_{proximal}$ Vph1NT$_{distal}$-Vph1CT	This study
*rav1*Δ SPVD	SF838 5Aα *rav1*Δ:: *URA3* Stv1NT$_{proximal}$Vph1NT$_{distal}$-Vph1CT	This study

603

604 **Table 1: Yeast strains used in this study**

605

Primer name	Sequence (5'→3')
SIV F	5'-GGCAGAGAAGGAGGAAGCGATTTTTCGCTCTGCTGAAATGGCTTTAGTC C-3'
SIV R	5'-CGAGCTTGCAAAGTAGCCAATTCGTCTCTTGGTATCCAACCTTCAGC-3'
Rav1Ura3F	5'-TTGAGAAAGTAAACAAACGTGCACACGCAAAGGTAGTTCTCATGTCATTGTGAGAGTGCACCACGCTTTTC-3'
Rav1Ura3R	5'-CAGAGTCGTTTGGCGCTTTTGGAGTTAAATTCTCTTTATGCTGAGAATATGAAGGAGAGAGTTTTGCTGGCCGCATCTTCT-3'
Vph1NT 5' BamH1	5'- GCGGATCCATGGCAGAGAAGGAGGAAGCG-3'
Vph1NT 3'FLAG	5'-CTACTTGTCATCGTCGTCCTTGTAGTCATCCAGGACTTGGATAATGGATGGGACATCAATACCCAATCTTGCGAT-3'
Stv1NT 133F	5'-GGAAGAAAGATTGATTCAATTAGATGAATCTTTAGATAGCCTT-3'
Stv1NT 324R	5'-GGCATATAAGGCATATAATTCACTTTCTAAAGTTTGTTCGGTAGTATCCAGG-3'
Vph1NT 124F	5'CGAATCCCGTGCAAGGCAAATGGAGGATGCAACCGATCAAATT-3'
Vph1NT 294R	5'-AACGAGCAGTTCTGTGTGTAAAGTGGTAGAAGTGGTTTTCAAAAC-3'
W83 Vph1F	5'- AAG AAA CAC GAT ATT AAG CTC TAC TGG AAG TAT ATT TTA CAT GAA GGA GAC ACG GAC AAA TAT TTG GAC GGC TCA GGT GAA-3'
Stv1W83Vph1R	5'-CGCCTTTTCACGGGTAACATCTTGGAACCAAGAGTCCAATTCTTTGGC-3'

606

607 **Table 2: Oligonucleotides used in this study**

608

609 **REFERENCES**

610 Banerjee, S., Clapp, K., Tarsio, M., & Kane, P. M. (2019). Interaction of the late endo-lysosomal
611 lipid PI(3,5)P2 with the Vph1 isoform of yeast V-ATPase increases its activity and
612 cellular stress tolerance. *J Biol Chem*, *294*(23), 9161-9171.
613 https://doi.org/10.1074/jbc.RA119.008552
614 Banerjee, S., & Kane, P. M. (2017). Direct interaction of the Golgi V-ATPase a-subunit isoform
615 with PI(4)P drives localization of Golgi V-ATPases in yeast. *Mol Biol Cell*, *28*(19), 2518-
616 2530. https://doi.org/10.1091/mbc.E17-05-0316
617 Benlekbir, S., Bueler, S. A., & Rubinstein, J. L. (2012). Structure of the vacuolar-type ATPase
618 from Saccharomyces cerevisiae at 11-A resolution. *Nat Struct Mol Biol*, *19*(12), 1356-
619 1362. https://doi.org/10.1038/nsmb.2422
620 Bonangelino, C. J., Nau, J. J., Duex, J. E., Brinkman, M., Wurmser, A. E., Gary, J. D., Emr, S.
621 D., & Weisman, L. S. (2002). Osmotic stress-induced increase of phosphatidylinositol
622 3,5-bisphosphate requires Vac14p, an activator of the lipid kinase Fab1p. *J Cell Biol*,
623 *156*(6), 1015-1028. https://doi.org/10.1083/jcb.200201002
624 Breton, S., & Brown, D. (2013). Regulation of luminal acidification by the V-ATPase.
625 *Physiology (Bethesda)*, *28*(5), 318-329. https://doi.org/10.1152/physiol.00007.2013
626 Casey, J. R., Grinstein, S., & Orlowski, J. (2010). Sensors and regulators of intracellular pH. *Nat*
627 *Rev Mol Cell Biol*, *11*(1), 50-61. https://doi.org/10.1038/nrm2820
628 Chandra, M., Chin, Y. K., Mas, C., Feathers, J. R., Paul, B., Datta, S., Chen, K. E., Jia, X., Yang,
629 Z., Norwood, S. J., Mohanty, B., Bugarcic, A., Teasdale, R. D., Henne, W. M., Mobli,
630 M., & Collins, B. M. (2019). Classification of the human phox homology (PX) domains
631 based on their phosphoinositide binding specificities. *Nat Commun*, *10*(1), 1528.
632 https://doi.org/10.1038/s41467-019-09355-y
633 Collins, M. P., Stransky, L. A., & Forgac, M. (2020). AKT Ser/Thr kinase increases V-ATPase-
634 dependent lysosomal acidification in response to amino acid starvation in mammalian
635 cells. *J Biol Chem*, *295*(28), 9433-9444. https://doi.org/10.1074/jbc.RA120.013223
636 Couoh-Cardel, S., Milgrom, E., & Wilkens, S. (2015). Affinity Purification and Structural
637 Features of the Yeast Vacuolar ATPase Vo Membrane Sector. *J Biol Chem*, *290*(46),
638 27959-27971. https://doi.org/10.1074/jbc.M115.662494
639 Diakov, T. T., & Kane, P. M. (2010). Regulation of vacuolar proton-translocating ATPase
640 activity and assembly by extracellular pH. *J Biol Chem*, *285*(31), 23771-23778.
641 https://doi.org/10.1074/jbc.M110.110122
642 Doherty, R. D., & Kane, P. M. (1993). Partial assembly of the yeast vacuolar H(+)-ATPase in
643 mutants lacking one subunit of the enzyme. *J Biol Chem*, *268*(22), 16845-16851.
644 https://www.ncbi.nlm.nih.gov/pubmed/8344963
645 Eaton, A. F., Merkulova, M., & Brown, D. (2021). The H(+)-ATPase (V-ATPase): from proton
646 pump to signaling complex in health and disease. *Am J Physiol Cell Physiol*, *320*(3),
647 C392-C414. https://doi.org/10.1152/ajpcell.00442.2020
648 Finnigan, G. C., Cronan, G. E., Park, H. J., Srinivasan, S., Quiocho, F. A., & Stevens, T. H.
649 (2012). Sorting of the yeast vacuolar-type, proton-translocating ATPase enzyme complex
650 (V-ATPase): identification of a necessary and sufficient Golgi/endosomal retention signal
651 in Stv1p. *J Biol Chem*, *287*(23), 19487-19500. https://doi.org/10.1074/jbc.M112.343814
652 Forgac, M. (2007). Vacuolar ATPases: rotary proton pumps in physiology and pathophysiology.
653 *Nat Rev Mol Cell Biol*, *8*(11), 917-929. https://doi.org/10.1038/nrm2272

654 Forloni, M., Liu, A. Y., & Wajapeyee, N. (2019). Megaprimer Polymerase Chain Reaction
655 (PCR)-Based Mutagenesis. *Cold Spring Harb Protoc*, *2019*(6).
656 https://doi.org/10.1101/pdb.prot097824
657 Frattini, A., Orchard, P. J., Sobacchi, C., Giliani, S., Abinun, M., Mattsson, J. P., Keeling, D. J.,
658 Andersson, A. K., Wallbrandt, P., Zecca, L., Notarangelo, L. D., Vezzoni, P., & Villa, A.
659 (2000). Defects in TCIRG1 subunit of the vacuolar proton pump are responsible for a
660 subset of human autosomal recessive osteopetrosis. *Nat Genet*, *25*(3), 343-346.
661 https://doi.org/10.1038/77131
662 Gietz, R. D., & Schiestl, R. H. (2007). High-efficiency yeast transformation using the LiAc/SS
663 carrier DNA/PEG method. *Nat Protoc*, *2*(1), 31-34. https://doi.org/10.1038/nprot.2007.13
664 Huotari, J., & Helenius, A. (2011). Endosome maturation. *EMBO J*, *30*(17), 3481-3500.
665 https://doi.org/10.1038/emboj.2011.286
666 Hurtado-Lorenzo, A., Skinner, M., El Annan, J., Futai, M., Sun-Wada, G. H., Bourgoin, S.,
667 Casanova, J., Wildeman, A., Bechoua, S., Ausiello, D. A., Brown, D., & Marshansky, V.
668 (2006). V-ATPase interacts with ARNO and Arf6 in early endosomes and regulates the
669 protein degradative pathway. *Nat Cell Biol*, *8*(2), 124-136.
670 https://doi.org/10.1038/ncb1348
671 Jaskolka, M. C., & Kane, P. M. (2020). Interaction between the yeast RAVE complex and Vph1-
672 containing Vo sectors is a central glucose-sensitive interaction required for V-ATPase
673 reassembly. *J Biol Chem*. https://doi.org/10.1074/jbc.RA119.011522
674 Jaskolka, M. C., Winkley, S. R., & Kane, P. M. (2021). RAVE and Rabconnectin-3 Complexes
675 as Signal Dependent Regulators of Organelle Acidification. *Front Cell Dev Biol*, *9*,
676 698190. https://doi.org/10.3389/fcell.2021.698190
677 Jin, N., Jin, Y., & Weisman, L. S. (2017). Early protection to stress mediated by CDK-dependent
678 PI3,5P2 signaling from the vacuole/lysosome. *J Cell Biol*, *216*(7), 2075-2090.
679 https://doi.org/10.1083/jcb.201611144
680 Kane, P. M. (1995). Disassembly and reassembly of the yeast vacuolar H(+)-ATPase in vivo. *J*
681 *Biol Chem*, *270*(28), 17025-17032. https://www.ncbi.nlm.nih.gov/pubmed/7622524
682 Kane, P. M. (2006). The where, when, and how of organelle acidification by the yeast vacuolar
683 H+-ATPase. *Microbiol Mol Biol Rev*, *70*(1), 177-191.
684 https://doi.org/10.1128/MMBR.70.1.177-191.2006
685 Kane, P. M. (2012). Targeting reversible disassembly as a mechanism of controlling V-ATPase
686 activity. *Curr Protein Pept Sci*, *13*(2), 117-123.
687 https://www.ncbi.nlm.nih.gov/pubmed/22044153
688 Kane, P. M., Kuehn, M. C., Howald-Stevenson, I., & Stevens, T. H. (1992). Assembly and
689 targeting of peripheral and integral membrane subunits of the yeast vacuolar H(+)-
690 ATPase. *J Biol Chem*, *267*(1), 447-454. https://www.ncbi.nlm.nih.gov/pubmed/1530931
691 Kawasaki-Nishi, S., Bowers, K., Nishi, T., Forgac, M., & Stevens, T. H. (2001). The amino-
692 terminal domain of the vacuolar proton-translocating ATPase a subunit controls targeting
693 and in vivo dissociation, and the carboxyl-terminal domain affects coupling of proton
694 transport and ATP hydrolysis. *J Biol Chem*, *276*(50), 47411-47420.
695 https://doi.org/10.1074/jbc.M108310200
696 Kelley, L. A., Mezulis, S., Yates, C. M., Wass, M. N., & Sternberg, M. J. (2015). The Phyre2
697 web portal for protein modeling, prediction and analysis. *Nat Protoc*, *10*(6), 845-858.
698 https://doi.org/10.1038/nprot.2015.053

699 Li, S. C., Diakov, T. T., Rizzo, J. M., & Kane, P. M. (2012). Vacuolar H+-ATPase works in
700 parallel with the HOG pathway to adapt Saccharomyces cerevisiae cells to osmotic stress.
701 *Eukaryot Cell*, *11*(3), 282-291. https://doi.org/10.1128/EC.05198-11
702 Li, S. C., Diakov, T. T., Xu, T., Tarsio, M., Zhu, W., Couoh-Cardel, S., Weisman, L. S., & Kane,
703 P. M. (2014). The signaling lipid PI(3,5)P(2) stabilizes V(1)-V(o) sector interactions and
704 activates the V-ATPase. *Mol Biol Cell*, *25*(8), 1251-1262.
705 https://doi.org/10.1091/mbc.E13-10-0563
706 Liu, M., Tarsio, M., Charsky, C. M., & Kane, P. M. (2005). Structural and functional separation
707 of the N- and C-terminal domains of the yeast V-ATPase subunit H. *J Biol Chem*,
708 *280*(44), 36978-36985. https://doi.org/10.1074/jbc.M505296200
709 Lowry, O. H., Rosebrough, N. J., Farr, A. L., & Randall, R. J. (1951). Protein measurement with
710 the Folin phenol reagent. *J Biol Chem*, *193*(1), 265-275.
711 https://www.ncbi.nlm.nih.gov/pubmed/14907713
712 Lu, M., Ammar, D., Ives, H., Albrecht, F., & Gluck, S. L. (2007). Physical interaction between
713 aldolase and vacuolar H+-ATPase is essential for the assembly and activity of the proton
714 pump. *J Biol Chem*, *282*(34), 24495-24503. https://doi.org/10.1074/jbc.M702598200
715 Manolson, M. F., Proteau, D., Preston, R. A., Stenbit, A., Roberts, B. T., Hoyt, M. A., Preuss,
716 D., Mulholland, J., Botstein, D., & Jones, E. W. (1992). The VPH1 gene encodes a 95-
717 kDa integral membrane polypeptide required for in vivo assembly and activity of the
718 yeast vacuolar H(+)-ATPase. *J Biol Chem*, *267*(20), 14294-14303.
719 https://www.ncbi.nlm.nih.gov/pubmed/1385813
720 Manolson, M. F., Wu, B., Proteau, D., Taillon, B. E., Roberts, B. T., Hoyt, M. A., & Jones, E.
721 W. (1994). STV1 gene encodes functional homologue of 95-kDa yeast vacuolar H(+)-
722 ATPase subunit Vph1p. *J Biol Chem*, *269*(19), 14064-14074.
723 https://www.ncbi.nlm.nih.gov/pubmed/7514599
724 Mazhab-Jafari, M. T., Rohou, A., Schmidt, C., Bueler, S. A., Benlekbir, S., Robinson, C. V., &
725 Rubinstein, J. L. (2016). Atomic model for the membrane-embedded VO motor of a
726 eukaryotic V-ATPase. *Nature*, *539*(7627), 118-122. https://doi.org/10.1038/nature19828
727 McCartney, A. J., Zhang, Y., & Weisman, L. S. (2014). Phosphatidylinositol 3,5-bisphosphate:
728 low abundance, high significance. *Bioessays*, *36*(1), 52-64.
729 https://doi.org/10.1002/bies.201300012
730 Oot, R. A., Couoh-Cardel, S., Sharma, S., Stam, N. J., & Wilkens, S. (2017). Breaking up and
731 making up: The secret life of the vacuolar H(+) -ATPase. *Protein Sci*, *26*(5), 896-909.
732 https://doi.org/10.1002/pro.3147
733 Oot, R. A., & Wilkens, S. (2012). Subunit interactions at the V1-Vo interface in yeast vacuolar
734 ATPase. *J Biol Chem*, *287*(16), 13396-13406. https://doi.org/10.1074/jbc.M112.343962
735 Parra, K. J., & Kane, P. M. (1998). Reversible association between the V1 and V0 domains of
736 yeast vacuolar H+-ATPase is an unconventional glucose-induced effect. *Mol Cell Biol*,
737 *18*(12), 7064-7074. https://www.ncbi.nlm.nih.gov/pubmed/9819393
738 Parra, K. J., Keenan, K. L., & Kane, P. M. (2000). The H subunit (Vma13p) of the yeast V-
739 ATPase inhibits the ATPase activity of cytosolic V1 complexes. *J Biol Chem*, *275*(28),
740 21761-21767. https://doi.org/10.1074/jbc.M002305200
741 Paulo, J. A., O'Connell, J. D., Gaun, A., & Gygi, S. P. (2015). Proteome-wide quantitative
742 multiplexed profiling of protein expression: carbon-source dependency in Saccharomyces
743 cerevisiae. *Mol Biol Cell*, *26*(22), 4063-4074. https://doi.org/10.1091/mbc.E15-07-0499

744 Pettersen, E. F., Goddard, T. D., Huang, C. C., Couch, G. S., Greenblatt, D. M., Meng, E. C., &
745 Ferrin, T. E. (2004). UCSF Chimera--a visualization system for exploratory research and
746 analysis. *J Comput Chem*, *25*(13), 1605-1612. https://doi.org/10.1002/jcc.20084
747 Roh, S. H., Stam, N. J., Hryc, C. F., Couoh-Cardel, S., Pintilie, G., Chiu, W., & Wilkens, S.
748 (2018). The 3.5-A CryoEM Structure of Nanodisc-Reconstituted Yeast Vacuolar ATPase
749 Vo Proton Channel. *Mol Cell*, *69*(6), 993-1004 e1003.
750 https://doi.org/10.1016/j.molcel.2018.02.006
751 Sennoune, S. R., Bakunts, K., Martinez, G. M., Chua-Tuan, J. L., Kebir, Y., Attaya, M. N., &
752 Martinez-Zaguilan, R. (2004). Vacuolar H+-ATPase in human breast cancer cells with
753 distinct metastatic potential: distribution and functional activity. *Am J Physiol Cell*
754 *Physiol*, *286*(6), C1443-1452. https://doi.org/10.1152/ajpcell.00407.2003
755 Seol, J. H., Shevchenko, A., Shevchenko, A., & Deshaies, R. J. (2001). Skp1 forms multiple
756 protein complexes, including RAVE, a regulator of V-ATPase assembly. *Nat Cell Biol*,
757 *3*(4), 384-391. https://doi.org/10.1038/35070067
758 Sharma, S., Oot, R. A., & Wilkens, S. (2018). MgATP hydrolysis destabilizes the interaction
759 between subunit H and yeast V1-ATPase, highlighting H's role in V-ATPase regulation
760 by reversible disassembly. *J Biol Chem*, *293*(27), 10718-10730.
761 https://doi.org/10.1074/jbc.RA118.002951
762 Smardon, A. M., Diab, H. I., Tarsio, M., Diakov, T. T., Nasab, N. D., West, R. W., & Kane, P.
763 M. (2014). The RAVE complex is an isoform-specific V-ATPase assembly factor in
764 yeast. *Mol Biol Cell*, *25*(3), 356-367. https://doi.org/10.1091/mbc.E13-05-0231
765 Smardon, A. M., Nasab, N. D., Tarsio, M., Diakov, T. T., & Kane, P. M. (2015). Molecular
766 Interactions and Cellular Itinerary of the Yeast RAVE (Regulator of the H+-ATPase of
767 Vacuolar and Endosomal Membranes) Complex. *J Biol Chem*, *290*(46), 27511-27523.
768 https://doi.org/10.1074/jbc.M115.667634
769 Smardon, A. M., Tarsio, M., & Kane, P. M. (2002). The RAVE complex is essential for stable
770 assembly of the yeast V-ATPase. *J Biol Chem*, *277*(16), 13831-13839.
771 https://doi.org/10.1074/jbc.M200682200
772 Smith, A. N., Skaug, J., Choate, K. A., Nayir, A., Bakkaloglu, A., Ozen, S., Hulton, S. A.,
773 Sanjad, S. A., Al-Sabban, E. A., Lifton, R. P., Scherer, S. W., & Karet, F. E. (2000).
774 Mutations in ATP6N1B, encoding a new kidney vacuolar proton pump 116-kD subunit,
775 cause recessive distal renal tubular acidosis with preserved hearing. *Nat Genet*, *26*(1), 71-
776 75. https://doi.org/10.1038/79208
777 Stam, N. J., & Wilkens, S. (2017). Structure of the Lipid Nanodisc-reconstituted Vacuolar
778 ATPase Proton Channel: DEFINITION OF THE INTERACTION OF ROTOR AND
779 STATOR AND IMPLICATIONS FOR ENZYME REGULATION BY REVERSIBLE
780 DISSOCIATION. *J Biol Chem*, *292*(5), 1749-1761.
781 https://doi.org/10.1074/jbc.M116.766790
782 Su, Y., Blake-Palmer, K. G., Sorrell, S., Javid, B., Bowers, K., Zhou, A., Chang, S. H., Qamar,
783 S., & Karet, F. E. (2008). Human H+ATPase a4 subunit mutations causing renal tubular
784 acidosis reveal a role for interaction with phosphofructokinase-1. *Am J Physiol Renal*
785 *Physiol*, *295*(4), F950-958. https://doi.org/10.1152/ajprenal.90258.2008
786 Sumner, J. P., Dow, J. A., Earley, F. G., Klein, U., Jager, D., & Wieczorek, H. (1995).
787 Regulation of plasma membrane V-ATPase activity by dissociation of peripheral
788 subunits. *J Biol Chem*, *270*(10), 5649-5653. https://doi.org/10.1074/jbc.270.10.5649

789 Sun-Wada, G. H., Wada, Y., & Futai, M. (2003). Lysosome and lysosome-related organelles
790 responsible for specialized functions in higher organisms, with special emphasis on
791 vacuolar-type proton ATPase. *Cell Struct Funct*, *28*(5), 455-463.
792 https://doi.org/10.1247/csf.28.455
793 Vasanthakumar, T., Bueler, S. A., Wu, D., Beilsten-Edmands, V., Robinson, C. V., &
794 Rubinstein, J. L. (2019). Structural comparison of the vacuolar and Golgi V-ATPases
795 from Saccharomyces cerevisiae. *Proc Natl Acad Sci U S A*, *116*(15), 7272-7277.
796 https://doi.org/10.1073/pnas.1814818116
797 Zhao, J., Benlekbir, S., & Rubinstein, J. L. (2015). Electron cryomicroscopy observation of
798 rotational states in a eukaryotic V-ATPase. *Nature*, *521*(7551), 241-245.
799 https://doi.org/10.1038/nature14365

800